

## Chapter 5

# The influence of galaxy environment

So far, I have considered galaxy mergers & interactions, morphology and AGN as causes of quenching across the galaxy population. While it is abundantly clear that these processes can strongly affect the SFHs of galaxies, the density of a galaxy's environment is also thought to be a driver of galaxy evolution.

The galaxy environment as a cause of quenching was proposed due to the correlation of environmental density with morphology (Dressler, 1980; Smail et al., 1997; Poggianti et al., 1999; Postman et al., 2005; Bamford et al., 2009), colour (Butcher & Oemler, 1978; Pimbblet et al., 2002) and the quenched galaxy fraction (Kauffmann et al., 2003b; Baldry et al., 2006; Peng et al., 2012; Darvish et al., 2016). Star forming disc galaxies tend to be located in low-density environments with quiescent elliptical galaxies in more dense environments. Although these correlations were originally interpreted as causation, recent evidence from simulations suggests that quenching mechanisms driven by the environment may not be dominant in the galaxy lifecycle (Kimm et al., 2009, 2011; Hirschmann et al., 2014; Wang et al., 2014; Phillips et al., 2015). Perhaps instead, the correlation of increased galaxy quenched fractions with environment is due to a superposition of the effects of mergers, interactions and both mass and morphology quenching.

In order to isolate the cause of the density-morphology and density-SFR correlations, I need to observe how morphology and galaxy quenching timescales change in dense environments with different properties in comparison to the field. Here, I con-

sider the group environment, as this is a more typical environment for a galaxy than the relatively rare rich cluster environment (Carlberg, 2004). I construct a sample of both group and field galaxies and once again use STARPY to determine the quenching time and rate to describe a simple SFH for a galaxy given its photometry. However, dense environments are messy with many possible mechanisms at work, whose effects are difficult to disentangle.

I aim to determine the following: (i) How does the environment influence the detailed morphological structures of a galaxy? (ii) Is quenching which is directly caused by the environment occurring in galaxy groups?

## 5.1 Data and Methods

### 5.1.1 Group Identification

The construction of a robust cluster or group catalogue is a thesis in itself, with many studies attempting this across the SDSS (Merchán & Zandivarez, 2005; Miller et al., 2005; Berlind et al., 2006; Yang et al., 2007; Tago et al., 2008, 2010; Tinker et al., 2011; Muñoz-Cuartas & Müller, 2012; Tempel et al., 2014) and other large surveys (Tucker et al., 2000; Merchán & Zandivarez, 2002; Eke et al., 2004; Cucciati et al., 2010; Robotham et al., 2011; Knobel et al., 2012). The difficulties arise in removing projection effects, understanding the selection function used, covering large ranges in mass and redshift, and dealing with spectral fibre collisions (see the comprehensive review by Postman, 2002, for an in depth discussion). Various different methods have been employed to achieve robust cluster/group identification including clustering algorithms (e.g. Miller et al., 2005), galaxy colour modelling (Koester et al., 2007), adaptive filter halo modelling (Yang et al., 2005, 2007) and friends-of-friends algorithms (Goto, 2005b; Merchán & Zandivarez, 2005; Berlind et al., 2006).

Each group finding algorithm has to be tested for purity (how contaminated the groups are by non-members) and completeness (how often are true members excluded from a group). Campbell et al. (2015) compared the purity and completeness of two of the most frequently used group catalogues of Berlind et al. (2006, a friends-of-friends algorithm) and Yang et al. (2007, a halo modelling algorithm) and concluded that no sample could achieve perfect purity or completeness. Despite the different algorithms

employed to identify group galaxies, Campbell et al. found that the two catalogues are remarkably similar. The Yang et al. catalogue has however, higher purity of satellites at lower halo masses (i.e. the low halo mass groups are less contaminated by non-members). For this reason the Yang et al. catalogue is the most commonly used in environment studies using data from the SDSS (including Hoyle et al., 2011; Pasquali et al., 2012; Wetzel et al., 2014; Shankar et al., 2014; Lacerna et al., 2014; Knobel et al., 2015; Fitzpatrick & Graves, 2015; Lan et al., 2016; Woo et al., 2016; Bluck et al., 2016; Weigel et al., 2016), but I find that when cross matched with the GZ2-GALEX sample (with a  $3''$  search radius) only 38 galaxies (of 176,604 possible galaxies) which belong to a group with 2 or more members are identified. This is most likely due to the necessity for GALEX NUV photometry in this study. The majority of NUV emission comes from massive, short lived stars and so in the cluster environment which is dominated by typical ‘red and dead’ quiescent galaxies, detecting NUV emission is less likely.

Instead I use the Berlind et al. (2006) catalogue, which when cross matched with the GZ2-GALEX sample and limited to  $z < 0.1^1$ , gives 14,199 group galaxies with the number of group members,  $N_{\text{group}} \geq 2$ . Centrals were selected as the most massive galaxy in a group (as in Yang et al., 2007, 2009; Pasquali et al., 2010) with all other galaxies in a group designated as satellites.

The projected group-centric radius,  $R$ , of all satellite galaxies was calculated from the projected separations of the co-ordinates of a satellite from its central; this was then converted to kpc by using the observed spectroscopic redshift of the central galaxy. In order to compare groups of different sizes, the virial radius is used as a normalisation factor to this projected group-centric radius. Here I use a proxy to the virial radius,  $R_{200}$  (see Navarro et al., 1995), the radius within which the group mass overdensity is 200 times the critical density,  $\rho_{\text{crit}}(z)$ , as defined by Finn et al. 2005:

$$200\rho_{\text{crit}}(z) = \frac{M_{cl}}{\frac{4}{3}\pi R_{200}^3}, \quad (5.1)$$

where  $M_{cl}$  is the mass of the group. Finn et al. then use the redshift dependance of the critical density and the virial mass to relate the line-of-sight velocity dispersion,

---

<sup>1</sup>To ensure GALEX completeness of the red sequence, unlike in Chapter 3; see Wyder et al. 2007; Yesuf et al. 2014

$\sigma_x$ , to the group mass so that  $R_{200}$  becomes:

$$R_{200} = 1.73 \left( \frac{\sigma_x}{1000 \text{ km s}^{-1}} \right) \cdot \frac{1}{\sqrt{\Omega_\Lambda + \Omega_o(1+z)^3}} h_{100}^{-1} \text{ Mpc}, \quad (5.2)$$

$\sigma_x$  is calculated for a group as the standard deviation of the velocity dispersions  $\sqrt{(v_i - \langle v_i \rangle)^2}$ . Here  $v_i$  are the proper velocities of each galaxy,  $i$  as defined in Danese et al. (1980):

$$v_i = c \cdot \frac{z_i - z_{\text{group}}}{1 + z_{\text{group}}}, \quad (5.3)$$

where  $z_{\text{group}}$  is the mean redshift of all the group members. Since most groups in the sample have low  $N_{\text{group}}$ , using the mean redshift for  $z_{\text{group}}$ , rather than the central galaxy redshift is most appropriate in this case. These calculations resulted in a sample of 3,468 centrals and 10,731 satellites within a projected group-centric radius range of  $0.02 < R/R_{200} < 24.9$  and  $z < 0.084$  which shall be referred to as the GZ2-BERLIND sample. Note that for a galaxy (central or satellite) to be included in the GZ2-BERLIND sample, the rest of its group does not. However the properties of that group are still retained by the included galaxy.

Unlike in previous Chapters, here I will specifically focus on galaxies that are below the star forming sequence (SFS) in order to simplify the analysis (see Section 5.2.3). I therefore select a subsample of the GZ2-BERLIND galaxies that are  $1\sigma$  below the SFS, giving 4,629 satellite and 2,314 central galaxies which will collectively be referred to as the GZ2-GROUP sample. These galaxies are shown in the panels of Figure 5.1 and can be seen to lie below the SFS.

I also compare the GZ2-BERLIND and GZ2-GROUP samples with a measurement of the projected neighbour density from Baldry et al. (2006),  $\Sigma_N = N/4\pi d_N^2$ , where  $d_N$  is the distance to the  $N^{\text{th}}$  nearest neighbour.  $\Sigma$  is a more direct probe of the local density of a galaxy's environment, and although it does not allow for the identification of groups and their properties, it is still a useful probe of the local density inside a group (see Muldrew et al., 2012, for a comparison of various environment parameterisations).

In this work I use the estimates of Bamford et al. (2009) who calculated the local galaxy density,  $\Sigma$ , determined by averaging  $\log \Sigma_N$  for  $N = 4$  and  $N = 5$  by the method outlined in Baldry et al. (2006), for the entirety of the GZ1 sample. 90% of the GZ2-BERLIND sample have  $\log \Sigma > -0.8$  (the threshold quoted by Baldry et al. 2006 above which non-field galaxies tend to be found), suggesting a purity of

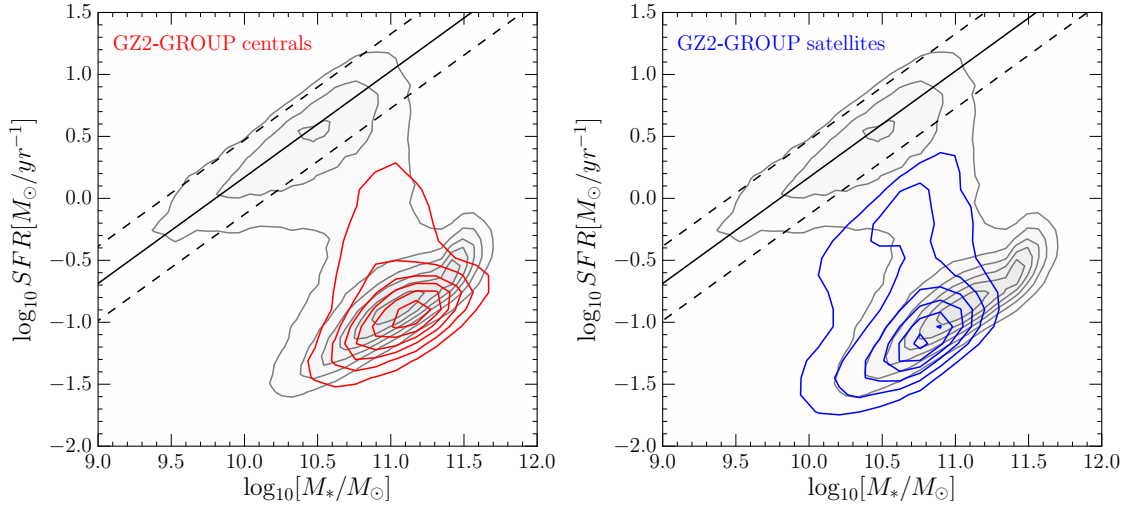


Figure 5.1: The stellar mass-SFR plane showing central (left; red contours) and satellite (right; blue contours) in the GZ2-GROUP sample. In both panels the entire SDSS sample from the MPA-JHU catalogue is shown by the grey contours. The definition of the SFMS from Peng et al. (2010) at  $\bar{z} = 0.053$  (solid line, the mean redshift of the GZ2-GROUP sample) with  $\pm 1\sigma$  (dashed lines) is shown.

$\sim 90\%$  for the GZ2-BERLIND sample. The distributions of  $\log \Sigma$  for star forming and quenching/quenched centrals and satellites in the GZ2-BERLIND sample are shown in Figure 5.2. Star forming galaxies tend to reside in less dense local environments than their quenching/quenched counterparts. The satellite galaxies as a whole also seem to occupy denser local environments than centrals, however on investigation this seems to arise because the satellites in the GZ2-BERLIND sample reside in groups with larger  $N_{group}$  than the centrals. This is to be expected given the definition of a satellite galaxy.

### 5.1.2 Field sample

I constructed a sample of field galaxies for use as a control sample to the GZ2-GROUP sample. For all galaxies in the GZ2-GALEX sample, I calculated the smallest projected group-centric radii,  $R/R_{200}$ , from each of the central galaxies in the Berlind et al. (2006) catalogue (regardless of whether the central was included in the GZ2-BERLIND sample) and selected candidate field galaxies as those with (i)  $R/R_{200} > 25$  and (ii)  $\log \Sigma < -0.8$  (the threshold on the local environment density which selects field

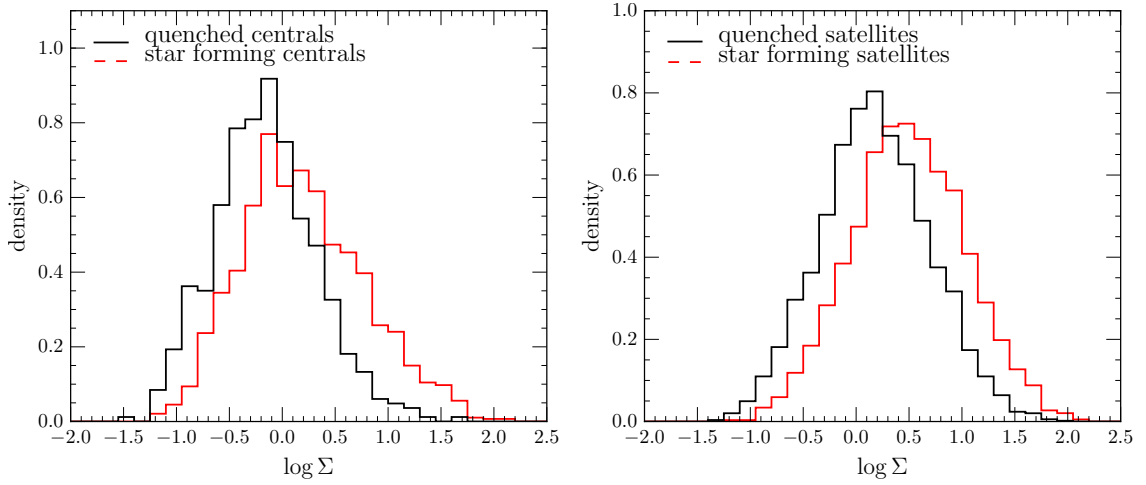


Figure 5.2: Local environment density,  $\log \Sigma$ , distributions of star forming (black) and quenching/quenched (red) central (left) and satellite (right) galaxies in the GZ2-GROUP sample.

galaxies as defined by Baldry et al., 2006). I chose to use both of these environmental density measures to ensure a pure sample of candidate field galaxies.

This sample of field galaxy candidates was then matched in redshift and stellar mass firstly to the central galaxies of the GZ2-GROUP sample to give 2,309 field galaxies with  $z < 0.084$ . In this work I shall focus on galaxies which are either quenching or quenched and are more than  $1\sigma$  below the SFS and so the same constraints must be placed on this field control sample. This encompasses 1,596 field galaxies with  $z < 0.084$  which will be referred to as the GZ2-CENT-FIELD-Q sample. It will be used as a control sample when investigating the trends with central galaxy properties of the inferred quenching parameters. The redshift distribution of the GZ2-CENT-FIELD-Q sample is shown in comparison to the distribution of central galaxies in the GZ2-GROUP sample in the left panel of Figure 5.3.

Secondly, the field galaxy candidates were then matched in redshift and stellar mass to the satellite galaxies of the GZ2-GROUP sample to give 5,004 field galaxies with  $z < 0.084$  which will be referred to as the GZ2-SAT-FIELD sample. These galaxies in the GZ2-SAT-FIELD sample will be used as a control when investigating the morphological trends of satellite galaxies with environment. Note that the sample is not restricted to being  $1\sigma$  below the SFS in this case. 237 galaxies are found in both the GZ2-CENT-FIELD-Q and GZ2-SAT-FIELD samples. The redshift distribution

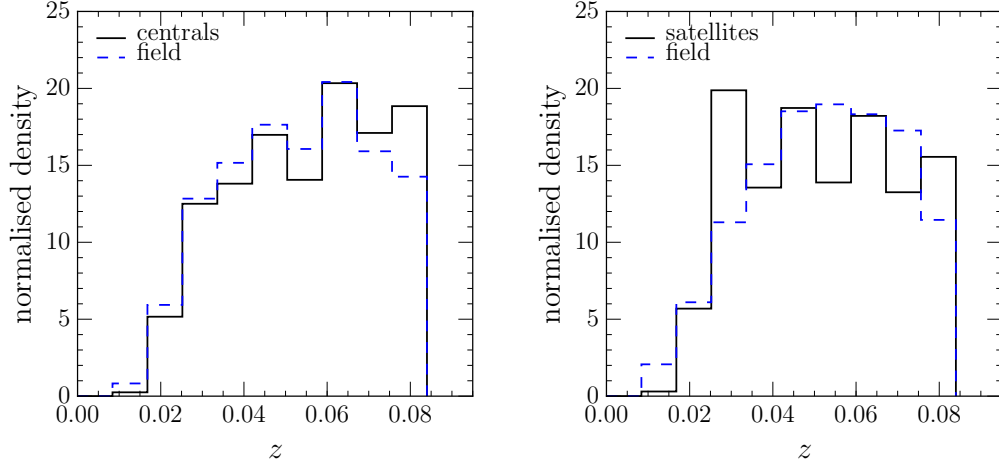


Figure 5.3: Redshift distributions of central (left) and satellite galaxies (right) in the GZ2-GROUP sample (black solid line) in comparison the redshift matched GZ2-CENT-FIELD-Q (left; blue dashed line) and GZ2-SAT-FIELD samples (right; blue dashed line).

of the GZ2-SAT-FIELD sample is shown in comparison to the distribution of satellite galaxies in the GZ2-GROUP sample in the right panel of Figure 5.3

We obtain SFRs and stellar velocity dispersions of galaxies for all of the field samples described above from the MPA-JHU catalogue (Kauffmann et al., 2003b; Brinchmann et al., 2004). Stellar masses were already calculated for the entire GZ2-GALEX sample using the optical photometry and the method outlined in Baldry et al. (2006, see Section 1.3.4).

### 5.1.3 Morphological fractions

I once again utilise the GZ2 vote fraction to quantify the morphology of galaxies in the GZ2-GROUP sample, in order to investigate the morphological trends with group radius. As in previous Chapters, I shall utilise  $p_{\text{disc}}$  and  $p_{\text{smooth}}$  but will also use  $p_{\text{bar}}$ ,  $p_{\text{bulge}}$  and  $p_{\text{merger}}$  to calculate the bar, bulge and merger fractions in the GZ2-GROUP sample respectively.

Fractions are calculated considering the number of barred (with  $p_{\text{bar}} > 0.5$ ; see Masters et al. 2011; Cheung et al. 2013) and bulged (with  $p_{\text{obvious or dominant}} > 0.5$  and  $p_{\text{none or noticeable}} > 0.5$  from Task 4 in the GZ2 decision tree shown in Figure 1.5)

galaxies over the number of disc galaxies ( $p_{\text{disc}} > 0.43$ ,  $p_{\text{edge\_on,no}} > 0.715$ ,  $N_{\text{edge\_on,no}} > 20$ ; see Table 1.1 in Chapter 1) in the GZ2-GROUP satellite sample. The merger fraction considers the number of merging galaxies (with  $p_{\text{merger}} > 0.4$ ; see Darg et al. 2010) over the number of galaxies in the GZ2-GROUP satellite sample.

## 5.2 Results

### 5.2.1 Mass dependance with radius

Since morphological features have been shown to be dependent on the stellar mass of a galaxy (e.g. the increase in the bar fraction with stellar mass; see Nair & Abraham, 2010b; Skibba et al., 2012), before investigating trends in the morphology with group radius in the GZ2-GROUP sample, the mass dependence on the group radius must be considered. This is shown in Figure 5.4. The mean stellar mass is roughly flat and consistent with the median field value with increasing group radius, until the most central group radius bin at  $R \sim 0.01 R_{200}$ . This trend is present for both morphologies, with early-type galaxies showing a larger increase in the average stellar mass. I note that if this inner bin at  $0.1R/R_{200}$  is ignored in the results that follow, my conclusions still hold.

### 5.2.2 Dependence of detailed morphological structure with environment

I perform an initial sanity check on the GZ2-GROUP sample by recreating the morphology-density relation of Dressler (1980, see Figure 1.3) in Figure 5.5, which shows the mean disc and smooth vote fractions as a function of group radius. The mean disc vote fraction decreases from the mean field value (blue line) within 1 virial radius, as the mean smooth vote fraction increases, in agreement with previous studies on the morphology-density relation (Dressler, 1980; Smail et al., 1997; Poggianti et al., 1999; Postman et al., 2005; Bamford et al., 2009). The extensive morphological classifications provided by GZ2 also allow for the investigation of how more detailed morphological structure is affected by the group environment.



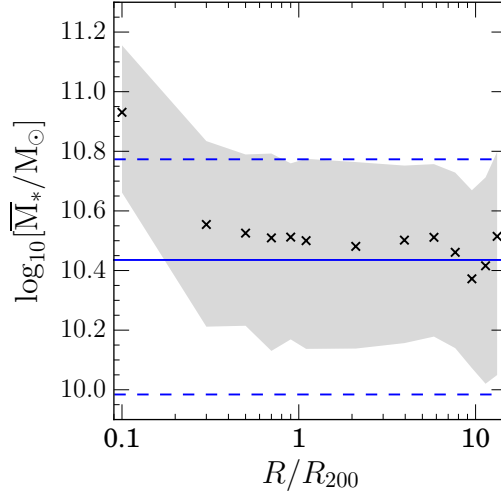


Figure 5.4: The average stellar mass as a function of radius from the group centre. The shaded regions show the  $\pm 1\sigma$  in each bin of  $R/R_{200}$ . The average stellar mass of the GZ2-SAT-FIELD sample is also shown (blue solid line) with  $\pm 1\sigma$  (blue dashed line).

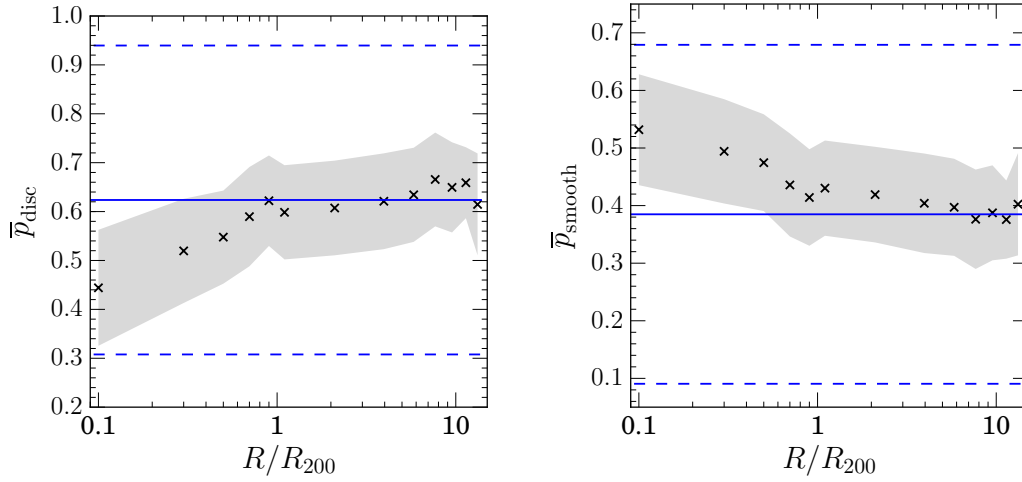


Figure 5.5: Mean GZ vote fraction for disc (top) and smooth (bottom) galaxies in the GZ2-GROUP sample binned in projected group-centric radius, normalised by  $R_{200}$ , a proxy for the virial radius of a group. The shaded region shows  $\pm 1\sigma$  on the mean vote fraction. The mean vote fraction of the GZ2-SAT-FIELD sample are also shown (blue solid lines) with  $\pm 1\sigma$  (blue dashed lines).

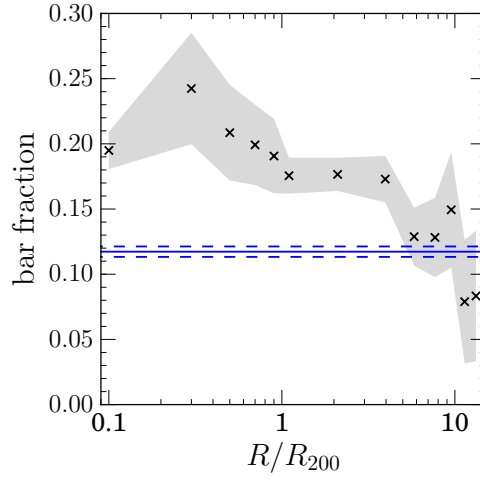


Figure 5.6: Bar fraction (number of barred disc galaxies over number of disc galaxies) in the GZ2-GROUP sample binned in projected group-centric radius, normalised by  $R_{200}$ , a proxy for the virial radius of a group. The shaded region shows  $\pm 1\sigma$  on the bar fraction. The bar fraction of the GZ2-SAT-FIELD sample is also shown (blue solid line) with  $\pm 1\sigma$  (blue dashed line).

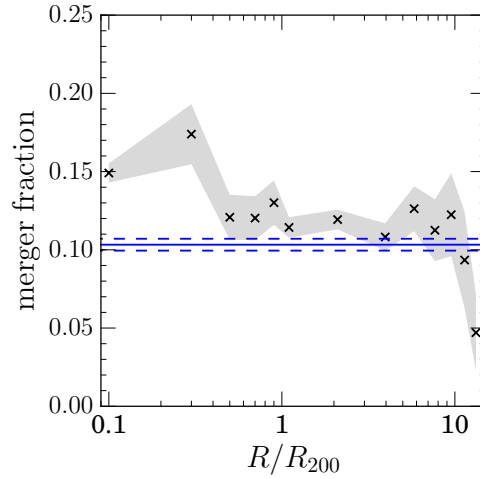


Figure 5.7: Merger fraction in the GZ2-GROUP sample binned in projected group-centric radius, normalised by  $R_{200}$ , a proxy for the virial radius of a group. The shaded region shows  $\pm 1\sigma$  on the merger fraction. The merger fraction of the GZ2-SAT-FIELD sample is also shown (blue solid line) with  $\pm 1\sigma$  (blue dashed line).

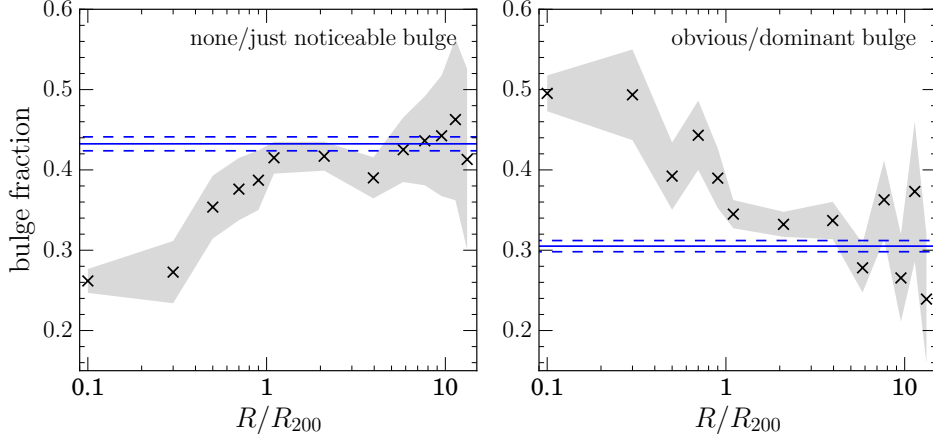


Figure 5.8: Fraction of galaxies with none/just noticeable bulge classifications (left) and with obvious/dominant bulge classifications (right) in the GZ2-GROUP sample binned in projected group-centric radius, normalised by  $R_{200}$ , a proxy for the virial radius of a group. The shaded regions shows  $\pm 1\sigma$  on the bulge fractions. The bulge fractions of the GZ2-SAT-FIELD sample are also shown (blue solid lines) with  $\pm 1\sigma$  (blue dashed lines).

Figure 5.6 shows how the bar fraction (number of barred disc galaxies over the number of disc galaxies; see Section 5.1.3) with decreasing group-centric radius increases significantly over the field fraction (blue solid line). Figure 5.7 shows how the merger fraction does not significantly deviate from the field fraction (blue solid line) except for galaxies found within a virial radius. As discussed in Chapter 4, mergers are thought to grow bulges and so similarly, Figure 5.8 shows how the fraction of galaxies with obvious/dominant bulges increases over the field value in the inner regions of the group and the fraction of those with none/just noticeable bulges decreases below the field value within 1 virial radius.

### 5.2.3 Quenching histories in the group environment

The SFHs of all galaxies in both the GZ2-GROUP and GZ2-CENT-FIELD-Q samples were analysed using STARPY, providing the posterior probability distribution across the two-parameter space for an individual galaxy. Whereas in Chapters 3 & 4 the POPSTARPY method was then used to combine and weight the individual distributions to give an overall distribution representing the population of galaxies, due to the

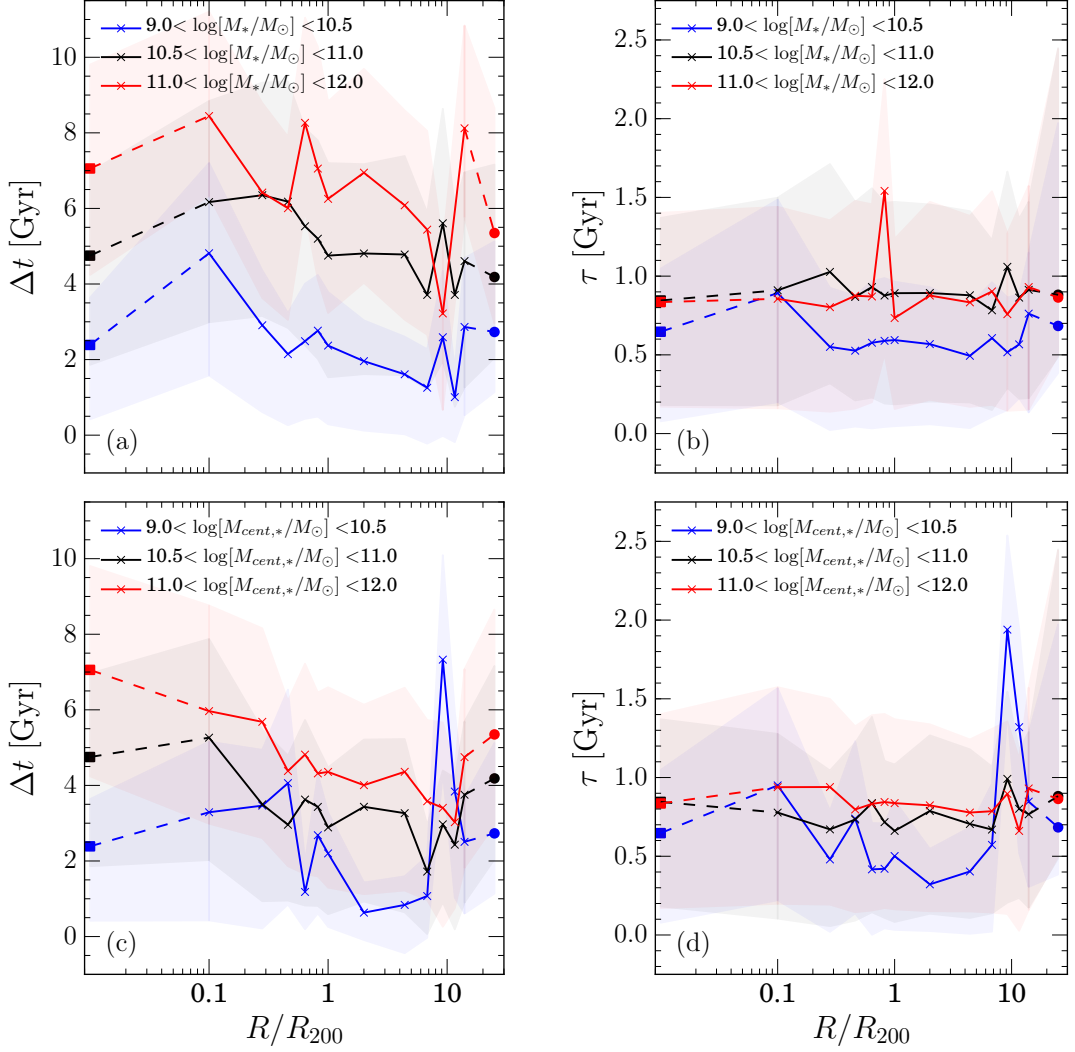


Figure 5.9: The time since quenching onset ( $\Delta t = t_{obs} - t_q$ ; left) and rate of quenching ( $\tau$ ; right) binned in group radius,  $R/R_{200}$ , for satellite galaxies (crosses) split into bins of stellar mass (top) and stellar mass of the corresponding central galaxy (bottom; a proxy for halo mass of a group). The corresponding values for central galaxies (squares, plotted at  $0.01R/R_{200}$ ) and galaxies in the GZ2-CENT-FIELD-Q sample (circles, plotted at  $25R/R_{200}$ ) are shown and connected by the dashed lines to help guide the eye. The shaded regions show the  $\pm 1\sigma$  on  $\Delta t$  and  $\tau$  in each bin of  $R/R_{200}$ .

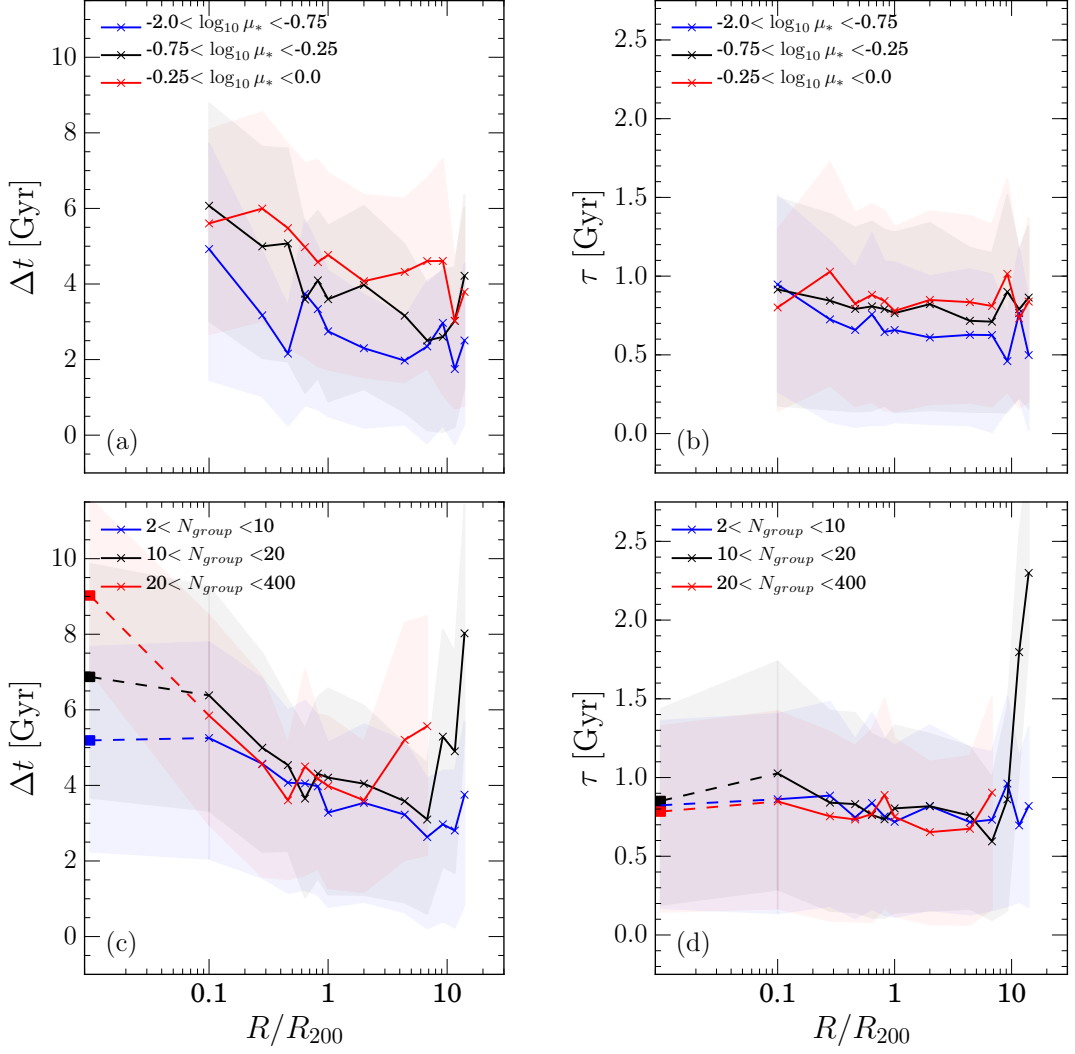


Figure 5.10: The time since quenching onset ( $\Delta t = t_{obs} - t_q$ ) and rate of quenching ( $\tau$ ; right) binned in group radius,  $R/R_{200}$ , for satellite galaxies (crosses) split into bins of number of group members ( $N_{group}$ , top) and stellar mass ratio ( $\mu_* = M_*/M_{cent,*}$ , bottom). The corresponding values for central galaxies (squares, plotted at  $0.01R/R_{200}$ ) and galaxies in the GZ2-CENT-FIELD-Q sample (circles, plotted at  $25R/R_{200}$ ) are shown, where possible, and connected by the dashed lines to help guide the eye. The shaded regions show the  $\pm 1\sigma$  on  $\Delta t$  and  $\tau$  in each bin of  $R/R_{200}$ .

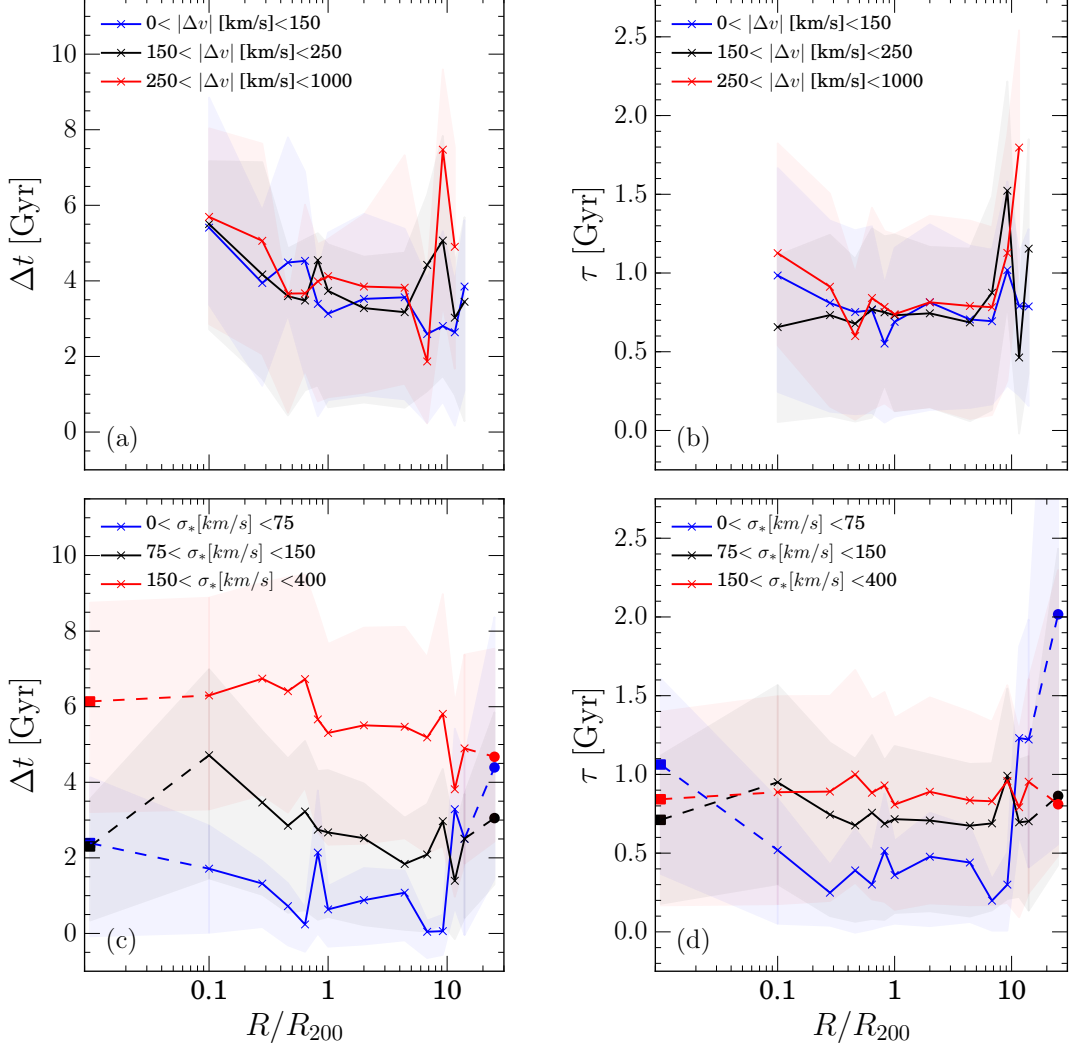


Figure 5.11: The time since quenching onset ( $\Delta t = t_{obs} - t_q$ ; left) and rate of quenching ( $\tau$ ; right) binned in group radius,  $R/R_{200}$ , for satellite galaxies (crosses) split by the absolute relative velocity of the satellite to its central galaxy ( $|\Delta v|$ , top) and stellar velocity dispersion ( $\sigma_*$ , bottom). The corresponding values for central galaxies (squares, plotted at  $0.01 R/R_{200}$ ) and galaxies in the GZ2-CENT-FIELD-Q sample (circles, plotted at  $25 R/R_{200}$ ) are shown, where possible, and connected to the satellite values by the dashed lines to help guide the eye. The shaded regions show the  $\pm 1\sigma$  on  $\Delta t$  and  $\tau$  in each bin of  $R/R_{200}$ .

complex nature of the group environment, the environmental effects will be washed out using this method. In this Chapter, I instead take the 50th percentile walker position of an individual posterior probability distribution to give the most likely quenching time,  $t_q$  and quenching rate,  $\tau$ , for each galaxy (shown by the solid blue lines in Figure 2.4).

This simplifies the output from STARPY for each galaxy from a probability distribution to just two values, with  $\pm 1\sigma$  uncertainties (shown by the dashed blue lines in Figure 2.4) which encompass the spread of the individual galaxy’s SFH posterior probability distribution. In this Chapter I will calculate the time since quenching onset,  $\Delta t$ , for a given galaxy by calculating  $\Delta t = t^{\text{obs}} - t_q$  (where  $t^{\text{obs}}$  is the age of the Universe at a galaxy’s observed redshift; see Section 2.1).

With the output from STARPY I can observe the trends in the time since quenching onset,  $\Delta t$ , and quenching rate,  $\tau$ , with group radius,  $R/R_{200}$ , for satellite galaxies and central galaxies in the GZ2-GROUP sample, compared with galaxies in the GZ2-CENT-FIELD-Q sample. This is shown in Figures 5.9 - 5.11 wherein the GZ2-GROUP galaxies are binned by stellar mass (Figures 5.9a-b), halo mass (Figures 5.9c-d), mass ratio (Figures 5.10a-b), number of group galaxies (Figures 5.10c-d), relative velocity (Figures 5.11a-b) and stellar velocity dispersion (Figures 5.11c-d). All bin thresholds were chosen to give approximately the same number of galaxies in each bin.

Across all the left panels in Figures 5.9 - 5.11 a general trend for increasing time since quenching onset with group radius can be seen. As in Figures 5.5–5.8 significant differences from the mean field values arise at radii less than a virial radius. However, no trend with group radius is seen for the rate at which quenching occurs for satellites in the GZ2-GROUP sample (right panels Figures 5.9 - 5.11). This suggests that whatever mechanisms causes quenching in a group will do so at the same rate in both the dense inner and sparse outer regions.

In Figure 5.9a the GZ2-GROUP sample is split by stellar mass,  $M_*$ , and a clear trend for increasing  $\Delta t$  with increasing stellar mass for satellite, central and field galaxies can be seen. However, this trend is less apparent for the rate of quenching seen in Figure 5.9b. The central galaxies (shown by the square points at  $\sim 0.01R/R_{200}$ ) appear to have quenched more recently than the inner satellites (at  $\sim 0.1R/R_{200}$ ) of the same mass but have done so at the same quenching rate.

In the bottom panels of Figure 5.9 I split the GZ2-GROUP sample by halo mass by using the stellar mass of the corresponding central galaxy of a group,  $M_{c,*}$  as a proxy. I find a clear trend for increasing time since quenching onset with increasing halo mass for satellite, central and field galaxies (Figure 5.9c) but once again this trend is less apparent for the rate of quenching (Figure 5.9d) suggesting the halo mass does not affect which quenching mechanism acts upon either central or satellite galaxies.

To account for the effects of conformity, whereby satellites of higher mass tend to be found in higher mass halos (Weinmann et al., 2006; Kauffmann et al., 2013; Hearin et al., 2015; Hatfield & Jarvis, 2016), I also split the satellites of the GZ2-GROUP sample by the stellar mass ratio of the satellite to its central galaxy,  $\mu_* = M_*/M_{cent,*}$ , in the top panels of Figure 5.10.  $\Delta t$  increases more steeply with group radius (particularly within  $\sim$  a virial radius; Figure 5.10a) for satellite galaxies with much smaller masses than their group central ( $-2.0 < \log_{10} \mu_* < -0.75$ , shown by the blue curve). Once again this is not the case for the rate that quenching occurs, as shown in Figure 5.10b.

Another property of the group which is expected to affect the satellite quenching histories is the number of group members,  $N_{group}$ , which should be roughly correlated with a satellite’s local density in a group. The bottom panels of Figure 5.10 show that there is no trend with time since quenching onset or rate of quenching with increasing  $N_{group}$  for satellite galaxies. The central galaxies (shown by the square points at  $\sim 0.01R/R_{200}$ ) however, do show a trend for increasing time since quenching as the number of group galaxies increases (Figure 5.10c), but the rate at which they quench is the same (Figure 5.10d) suggesting the mechanism by which this occurs is the same for all centrals regardless of halo mass.

In the top panels of Figure 5.11 the GZ2-GROUP satellite galaxies are split into bins of their relative velocity to their central galaxies, i.e. the velocity at which they move through the dense group environment. There is no trend with either time since onset of quenching (Figure 5.11a) or rate of quenching (Figure 5.11b) with increasing relative velocity for galaxies in the GZ2-GROUP sample. This suggests that whatever quenching mechanism is occurring in groups, it is not correlated with the velocity at which satellites move through the dense environment.

The bottom panels of Figure 5.11 show the trend with group radius for the GZ2-GROUP satellites when split into bins of galaxy stellar velocity dispersion  $\sigma_*$  (note



Table 5.1: Summary of results shown in Figures 5.9-5.11 denoting whether there is,  $\checkmark$ , or isn't,  $\times$ , a trend with  $\Delta t$  when the GZ2-GROUP satellite galaxies are split by the stated property.

	$M_*$	$M_{\text{cent},*}$	$\mu_*$	$N_{\text{group}}$	$ \Delta v $	$\sigma_*$
Shown in Figure	5.9a	5.9c	5.10a	5.10c	5.11a	5.11c
Trend with $\Delta t$ when split by ...?	$\checkmark$	$\checkmark$	$\checkmark$	$\times$	$\times$	$\checkmark$

that this is not the velocity dispersion of the group) which is often used as a proxy for the galaxy potential. The stellar velocity dispersion show the largest trend in  $\Delta t$  (Figure 5.11c) for satellite galaxies of all of the group or satellite galaxy properties studied, with galaxies with the smallest stellar velocity dispersions having quenched more recently. Although this trend is less apparent in Figure 5.11d for the rate that quenching occurs with  $\sigma_*$ , it is the largest trend seen across the right panels of Figures 5.9-5.11. Also, field galaxies (shown by the circles at  $\sim 25R/R_{200}$ ) with low velocity dispersions are seen to quench at much slower rates than their satellite counterparts. This suggests that the rapid quenching observed for the low stellar velocity dispersion satellites is directly caused by the environment.

The results shown in Figures 5.9-5.11 are summarised in Table 5.1.

## 5.3 Discussion

I shall now consider the results presented in Section 5.2 in the context of possible quenching mechanisms which could be responsible.

### 5.3.1 The role of mergers as quenching mechanisms in the group environment

The merger classification in GZ2 has been shown to preferentially identify major mergers (Darg et al., 2010); while bulge formation in disc galaxies is often associated with evolutionary histories driven by minor mergers (Croton et al., 2006; Tonini et al., 2016). Although we see evidence for an enhanced merger fraction in the inner regions of the group environment in Figure 5.7, the bulge fractions in Figure 5.8 vary much more significantly from the field value than the merger fraction. This suggests that

minor mergers may be more dominant than major mergers for satellites in the group environment, particularly at  $R/R_{200} > 0.5$ .

If mergers are a dominant evolutionary mechanism for satellite galaxies, as the morphological evidence in Figures 5.7 & 5.8 suggests, we would expect to see a difference in the quenching histories of satellites residing in groups with a larger number of members. However, the bottom panels of Figure 5.10 show there is no trend with time since quenching onset or rate of quenching with increasing  $N_{group}$  for the satellite galaxies. This suggests that mergers are not the dominant quenching mechanism for satellite galaxies, but that whatever mechanism is the cause of the quenching occurs at the same rate irrespective of group size.

Central galaxies however, do show a trend for increasing time since quenching with increasing  $N_{group}$  (square points at  $0.01R/R_{200}$  in Figure 5.10c) occurring at a rate of  $\tau \sim 1\text{Gyr}$  (which as discussed in Chapter 3, was attributed to mergers and galaxy interactions which could transform a galaxy’s morphology). Therefore, the larger the number of group members, the more likely a central galaxy has a history dominated by mergers. This is in agreement with the findings of Lin et al. (2010), Ellison et al. (2010), Lidman et al. (2013) and McIntosh et al. (2008). The latter found in a sample of local groups and clusters that half of the mergers they identified involved the central galaxy. Liu et al. (2009) also found that the fraction of merging centrals increases with the richness of a cluster (a measure of the number of galaxies within  $1h^{-1}\text{Mpc}$  of the central galaxy).

This idea is supported by the result in Figure 5.9a showing that centrals of a given mass have quenched more recently than the inner satellites (at  $\sim 0.1R/R_{200}$ ) of a given mass. This suggests that an episode of more recent star formation, such as a starburst, may have occurred in the central galaxies but not in the inner satellites. Mergers are thought to cause an energetic burst of star formation which can in turn quench the remnant galaxy (Hopkins et al., 2005; Treister et al., 2012; Pontzen et al., 2016, as discussed in Section 3.3.1). This result is also suggestive of a merger dominated history for central galaxies but not for satellite galaxies.

### 5.3.2 The role of mass quenching in the group environment

A trend is seen for increasing time since quenching with increasing stellar mass and velocity dispersion (a proxy or galaxy potential) for centrals, satellites and field galaxies in Figure 5.9a and Figure 5.11c respectively. This is suggestive of mass quenching occurring across the entire galaxy population irrespective of environmental density, supporting the work of Peng et al. (2010, 2012); Gabor et al. (2010) and Darvish et al. (2016).

### 5.3.3 The role of morphological quenching in the group environment

The increasing bar fraction toward the central group regions shown in Figure 5.6 (in agreement with Skibba et al., 2012), suggests that bars may be partly responsible for the relation between quenched fraction and environmental density. This is consistent with findings that show that bars themselves may be the cause of morphological quenching through the funnelling of gas toward the central regions of galaxies (Athanasoula, 1992b; Sheth et al., 2005) which is then used in star formation, exhausting the available gas<sup>2</sup>.

We must therefore consider whether the environment itself may play a role in triggering the disk instabilities which can produce a bar. Indeed harassment and tidal interactions, believed to be common in the group environment, have been shown to both promote and inhibit bar formation dependent on the stellar mass (Noguchi, 1988; Moore et al., 1996; Skibba et al., 2012). If the environment was indeed triggering a bar, then morphological quenching would be occurring in the group environment but indirectly due to environmental quenching. This suggests that the polarity between internal secular processes (‘nature’) and external environmental processes (‘nurture’) may not be as extreme as first thought, in agreement with Skibba et al. (2012).

---

<sup>2</sup>The gas which is funnelled to the centre by the bar may also be used to fuel an AGN. The AGN-environment connection has been extensively studied with conflicting results; (Miller et al., 2003; Pimbblet et al., 2013; Ehlert et al., 2014; de Souza et al., 2016, e.g. see). I attempted to study this in this investigation. However, only 204 satellites and 128 centrals of the GZ2-GROUP sample were identified as obscured Type 2 AGN using a BPT diagram. These low numbers of AGN mean that when split into bins of group radius we are well and truly dancing precariously on the low number statistics volcano and so no robust conclusions can be drawn.

### 5.3.4 The role of the environment in quenching

Across all panels of Figures 5.9-5.11 a trend for increasing time since quenching onset with decreasing group radius is present. I interpret this as environmentally driven mechanisms causing quenching at the same rate throughout the infall time of a galaxy in a group. Those galaxies closer in, fell into the group earlier and as they did so they started to quench, giving rise to a larger inferred  $\Delta t$ .

More massive halos are seen to have a greater impact on the star formation histories of their satellites than less massive halos in Figure 5.9c. The halo mass is correlated with both (i) the gravitational potential of the group and (ii) the temperature of the IGM, suggesting that an environmental quenching mechanism which is correlated with one or both of these properties is responsible for this result.

Higher mass halos have hotter intra group medium (IGM) temperatures (Shimizu et al., 2003; Del Popolo et al., 2005) which can have a greater impact on a galaxy through ram pressure stripping (RPS) of cold gas. Gunn & Gott (1972) define the ram pressure as:

$$\rho_{\text{IGM}} \cdot v^2 = 2\pi G \cdot \sigma_*(R) \cdot \sigma_g(R), \quad (5.4)$$

where  $\rho_{\text{IGM}}$  is the density of the IGM,  $\sigma_*(R)$  the star surface density,  $\sigma_g(R)$  the gas surface density of the galaxy disc and  $v$  the velocity of the galaxy through the IGM. Therefore if RPS is indeed a dominant environmental quenching mechanism we should see a trend in  $\Delta t$  with the velocity of a satellite relative to its central galaxy. However in Figure 5.11a we see that this is not the case. This therefore rules out RPS as the dominant environmental quenching mechanism, in support of the simulations of Emerick et al. (2016); Fillingham et al. (2016) which showed that RPS could only remove 40 – 60% of a satellite’s gas. and observations by McGee et al. (2014). However, this conclusion may be due to the stellar mass range spanned by the GZ2-GROUP satellite galaxies which all have  $M_* \geq 10^9 M_\odot$ , as simulations by Fillingham et al. (2016) suggest that RPS only becomes effective in lower mass satellites with  $M_* \leq 10^{8-9} M_\odot$ , in agreement with Hester (2006).

Above this mass threshold in the simulations of Fillingham et al. (2016), a ‘starvation’ (or strangulation) mode (Larson et al., 1980; Balogh et al., 2000) dominates, where a galaxy’s extended gaseous halo is removed causing a quench, as cold gas for use in star formation is no longer be fed from the extended halo. This idea is supported by observations by Peng et al. (2010) which show that strangulation is a

dominant mechanism for galaxies with  $M_* < 10^{11} M_\odot$  with a quenching timescale of 4 Gyr. Such a mechanism will be correlated with the galaxy potential, as galaxies with a lower potential will be most easily stripped of their halos. This is apparent in Figure 5.11d where satellites with lower velocity dispersion (a proxy for the galaxy potential) are more rapidly quenched than their higher velocity dispersion counterparts and those in the field. Such a starvation mechanism is also correlated with halo mass, for which similar trends in  $\Delta t$  are seen in Figure 5.9c. The dominant environmental quenching mechanism occurring in the group environment must therefore be correlated with the group potential. This suggests that satellite galaxies may be most affected by gravitationally driven environmental effects, such as starvation, thermal evaporation of the galaxy halo and galaxy harassment.

We can calculate an infall timescale for the satellite galaxies in the GZ2-GROUP sample. We can assume that galaxies begin their infall into a group at a radius of  $\sim 10R_{200}$  and stop infalling at  $\sim 0.1R_{200}$ <sup>3</sup>. The difference in the time since quenching onset,  $\Delta t$ , between these two locations in a group will provide an estimate for how long it takes a satellite to infall. This assumes (i) that the galaxy starts to quenching immediately when it enters the group and (ii) that the same environmentally driven quenching process is the only quenching mechanism affecting the satellites throughout their infall. I will define this property as  $\delta\Delta t = \Delta t_{0.1R_{200}} - \Delta t_{10R_{200}}$ . In Figure 5.10c the trend seen in  $\Delta t$  with group radius is the same regardless of the number of galaxies in the group, so this gives us an estimate for the average  $\Delta t$  in each group-centric radius bin across the satellite population. We can therefore estimate an average infall time of  $\delta\Delta t \sim 3$  Gyr for the GZ2-GROUP satellites. The rate of quenching occurring across the group radius in Figure 5.10d is  $\tau \sim 1$  Gyr (this is within the range of quenching rates theorised to cause a morphological change in Section 3.2.2) and so we can also estimate the average quenching timescale (i.e. the time taken to fully quench from the SFS to  $5\sigma$  below the SFS, as in Chapters 3 & 4) to be  $\sim 4$  Gyr for the GZ2-GROUP satellites.

This infall time and quenching timescale are in agreement with the estimates of Wetzel et al. (2013) who used a high resolution cosmological N-body simulation to track satellite galaxy orbits in SDSS groups and clusters and found quenching timescales of 2 – 6 Gyr. Using a similar method, Oman & Hudson (2016) derive an infall time of  $\sim 4$  Gyr and quenching timescales between 4 – 6 Gyr for galaxies in

---

<sup>3</sup>This assumes that galaxies will then merge with their central galaxy, however it is more likely that the satellite has a close pass with the central before it ‘backslashes’ into the group.

the mass range of the GZ2-GROUP sample. Similarly, Hahn et al. (2016) derive a total quenching timescale of  $\sim 4$  Gyr for satellite galaxies on infall into the group environment. However, the simulations by Fillingham et al. (2016) and Emerick et al. (2016) have shown that RPS cannot remove enough gas mass to completely quench a galaxy within  $\sim 2$  Gyr but can assist in reducing the starvation timescale so that galaxies can be quenched within the  $\sim 4$  Gyr quenching timescale calculated in this study. This suggests that although the effects of mechanisms correlating with the group potential are detectable in the quenching parameters of the GZ2-GROUP sample, this is only made possible by the constantly present, but less dominant effects of ram pressure stripping.

This conclusion, along with the discussion in Section 5.3.3 which concluded that morphological quenching may only be present in the group environment due to the influence of the environment itself, suggests that all mechanisms discussed here will affect a galaxy which is infalling through the group environment at some point in its lifetime,. A single mechanism may be more dominant in the evolution of an individual galaxy but to achieve the correlations between morphology, colour and quenched galaxy fraction with density observed across the entire population all mechanisms need to act in concert.

## 5.4 Conclusions

Using the Berlind et al. (2006) group catalog, I have constructed a sample of group galaxies in the SDSS which were cross matched with Galaxy Zoo 2 and GALEX in order to determine their most likely SFHs using STARPY. I have shown that although mass quenching, morphological quenching and mergers are all important mechanisms at work in quenching the galaxies in the group environment, the environment does play a role in quenching galaxies as they infall into the group. I have discussed the possibility that not one mechanism will dominate across the group population, with all mechanisms acting collaboratively. My findings are summarised as follows:

- (i) The bar, obvious bulge and merger fractions are all seen to increase above the field value in the inner regions of the groups of the GZ2-GROUP sample in Figures 5.6, 5.8 & 5.7 respectively.

- (ii) Mergers are the dominant quenching mechanism for central galaxies but not for satellite galaxies. Satellites may undergo a minor merger in the group environment but their effects are only discernible by their indirect effect on the bulge fraction (see Figure 5.8).
- (iii) Mass quenching is occurring across the entire GZ2-GROUP sample for centrals and satellites irrespective of the environmental density (see Figure 5.9a).
- (iv) Morphological quenching is occurring for GZ2-GROUP satellite galaxies as evidenced by the heightened bar fraction in the inner group regions (see Figure 5.6). However, this may be indirectly due to environmental quenching since galaxy interactions and harassment are believed to be able to trigger bars. This suggests the polarity between ‘nature’ vs. ‘nurture’ may not be as extreme as previously thought.
- (v) The environment does cause quenching across the GZ2-GROUP sample, as evidenced by the increase in the time since quenching with decreasing group radius seen across all left panels of Figures 5.9-5.11. The results in Figures 5.9a & 5.11c suggest that this is caused by a quenching mechanism correlated with the group potential, such as harassment, interactions and starvation, rather than the velocity of a satellite through the group, such as ram pressure stripping. This quenching occurs within an average quenching timescale of  $\sim 4$  Gyr from star forming to complete quiescence, after an average infall time of  $\sim 3$  Gyr.

It is apparent from the results presented in this Chapter that many quenching mechanisms are all occurring simultaneously in the group environment; therefore a superposition of all of the effects of these mechanisms is seen in the quenching histories of the GZ2-GROUP sample, which in turn gives rise to the morphology-density relation observed.